

Chemo - Structural Disorder in the kagomé spin $S = 1/2$ systems $\text{ZnCu}_3(\text{OH})_6\text{Cl}_2$ and $\text{YCu}_3(\text{OH})_6\text{Br}_2[\text{Br}_x(\text{OH})_{1-x}]$

Reinhard K. Kremer,¹ Sebastian Bette,¹ Jürgen Nuss,¹ and Pascal Puphal^{1,2,*}

¹Max-Planck-Institute for Solid State Research, Heisenbergstraße 1, 70569 Stuttgart, Germany

²2nd Physics Institute, University of Stuttgart, 70569 Stuttgart, Germany

(Dated: November 28, 2024)

By single crystal diffraction we characterize the chemo - structural disorder introduced by Zn - Cu site mixing in the kagomé spin $S = 1/2$ systems herbertsmithite $\text{ZnCu}_3(\text{OH})_6\text{Cl}_2$ and $\text{YCu}_3(\text{OH})_6\text{Br}_2[\text{Br}_x(\text{OH})_{1-x}]$. For an untwinned single crystal of herbertsmithite of composition $\text{Zn}_{0.95(1)}\text{Cu}_{2.99(3)}\text{O}_{5.9(1)}\text{H}_{5.8(1)}\text{Cl}_2$ we find substitution by Cu of the Zn atoms in the layers separating the kagomé layers as well as substantial Zn substitution for Cu in the kagomé layers. In $\text{YCu}_3(\text{OH})_6\text{Br}_2[\text{Br}_x(\text{OH})_{1-x}]$ site mixing disorder is present for intermediate x . Analogous to the Cl homologous system in crystals with $x = 1/3$ disorder is absent and a low-temperature structural transition emerges driven by strong magneto-phonon coupling as a release of frustration. Apart from this structural anomaly we find the physical properties of these crystals unchanged compared to intermediate x and closely resembling the Cl homologue where long-range magnetic order was observed.

I. INTRODUCTION

Low-dimensional materials with strong magnetic frustration, such as compounds containing decoupled anti-ferromagnetic kagomé layers, are prototypical candidates to search for an experimental realization of the quantum spin-liquid (QSL) phase [1, 2]. This long-sought unusual quantum state exhibits no static magnetic order, despite sizable exchange interactions. Rather, macroscopic entanglement and fractional excitations are expected. Cu-based systems with perfect kagomé layers of Cu^{2+} spin $S = 1/2$ cations are considered prime QSL candidates and have been strongly investigated in the past. One of the first systems for which clear experimental signatures of a QSL phase were observed is herbertsmithite with composition $\text{ZnCu}_3(\text{OH})_6\text{Cl}_2$ [3, 4]. Lately, the Zn-substituted barlowite, $\text{ZnCu}_3(\text{OH})_6\text{BrF}$, was proposed as another putative QSL candidate [5, 6].

Herbertsmithite $\text{ZnCu}_3(\text{OH})_6\text{Cl}_2$ represents the $x = 1$ endmember of the substitution series of $\text{Zn}_x\text{Cu}_{4-x}(\text{OH})_6\text{Cl}_2$ crystallizing in the space group $R\bar{3}m$ with ABC-type stacking of the kagomé layers along the c axis. The kagomé layers are well separated by triangular layers of nonmagnetic Zn-anions, centering non-distorted oxygen octahedra. The kagomé layers result by connecting strongly Jahn-Teller elongated CuO_4Cl_2 octahedra leaving the Cu^{2+} cations with a square planar oxygen coordination and Cl^- anions at the elongated apical sites of the coordination octahedra.

Very early on chemical and structural disorder, for example, induced by site mixing of magnetic and nonmagnetic ions, or deviations from the perfect kagomé arrangement were a controversial topic when discussing the magnetic properties of herbertsmithite [7, 8]. By using neutron powder diffraction on a deuterated herbertsmithite

sample assuming a Cu^{2+} to Zn^{2+} ratio of 3 : 1 and no vacant cation sites, de Vries *et al.* reported a 91:9% Cu : Zn occupancy of the kagomé sites corresponding to a 73% occupancy of the interlayer Zn sites [9, 10]. On the other hand, Freedman *et al.* investigated a crystal with composition $\text{Zn}_{0.85}\text{Cu}_{3.15}(\text{OH})_6\text{Cl}_2$ by anomalous x-ray scattering and detected Cu atoms at the Zn sites but concluded no Zn substitution of the Cu kagomé layer sites [11]. Lattice distortions due to a Jahn-Teller effect of the Cu^{2+} ions substituting for the interlayer Zn^{2+} cations were discussed by Han *et al.* [12]. By Cu^{2+} electron spin resonance Zorko *et al.* found evidence for magnetic defects whose response violates trigonal symmetry [13]. They even suggested a global structural distortion related to the formation of the spin-liquid ground state. Norman *et al.* recently investigated possible global symmetry lowering in herbertsmithite and pointed out that small perturbations could stabilize an anisotropic spin-liquid or a valence bond solid [14]. As a consequence of site mixing often intricate sample dependence of the magnetic properties of herbertsmithite samples is observed which makes an unequivocal assessment of the ground state properties extremely challenging and, indeed, gapped [12, 15] and nongapped ground states have been discussed [4, 15–17].

With $\text{A}^{n+}\text{Cu}_3(\text{OH})_6\text{Cl}_n$ ($n = 2, 3$) a new series of related compounds has been found with $\text{A}^{3+}\text{Cu}_3(\text{OH})_6\text{Cl}_3$ [18–20], realizing perfect kagomé layers in a kapellasite-type structure (AA-stacking), the structural polymorph of herbertsmithite. For $\text{YCu}_3(\text{OH})_{6+x}\text{Cl}_3$ long range magnetic order (LRO) below a transition temperature of 15 K was reported driven by a strong Dzyaloshinskii-Moriya (DM) interaction [21–24].

However, for $\text{A} = \text{Y}$ the compound is not stable against water, leading to Cl-OH substitution and phases with compositions of $\text{YCu}_3(\text{OH})_{6+x}\text{Cl}_{3-x}$ are formed, until the endmember $\text{Y}_3\text{Cu}_9(\text{OH})_{19}\text{Cl}_8$ for $x = 1/3$ is obtained [25]. This substitutional variant shows a distortion of the Cu lattice as Y atoms move out of the kagomé plane [25]

* puphal@fkf.mpg.de

creating two non-equivalent Cu sites and a unique magnetic model with three different nearest-neighbor exchange interactions is required [26]. For $Y_3Cu_9(OH)_{19}Cl_8$ chemical disorder-free crystals can be obtained which undergo LRO below 2.2 K, as spin waves were seen in inelastic neutron scattering, and fast damped oscillations in μ SR were detected [27]. Multimagnon modes were accessed by terahertz time-domain spectroscopy, further confirming LRO, and a 1/6 magnetization plateau was observed. [28] Finally, in 1H -NMR a clear peak of the spin-lattice relaxation rate T^{-1} was observed at T_N [29].

Notably, a blend of the two Y phases with an intermediate x can be synthesized where a partial occupancy of the Y atoms is present [19]. In Ref. 30 a mixture of the two phases was reported with a major fraction of the Y atoms out of the plane. Specific heat measurements revealed two distinct anomalies and an entropy release at both transitions [27]. Recent low-temperature crystal structure investigations on various kagomé systems revealed structural instabilities which induce distortions as seen, for example, in the herbertsmithite parent compound clinoatacamite [31, 32], as well as for barlowite, claringbullite [33], volborthite [34] and vesigneite [35] indicating it to be a prevalent structural motif at low temperatures. Similarly, for $Y_3Cu_9(OH)_{19}Cl_8$ crystals as evidenced by thermal expansion and specific heat measurements a 33 K structural anomaly has been seen, which is suppressed in powder samples [27]. These low temperature distortions are attributed to enhanced magnetoelastic coupling, if the energies of magnetic interactions and phonons coincide, as was shown, for $Y_3Cu_9(OH)_{19}Cl_8$ in detailed phonon investigations by ellipsometry studies [36]. In polycrystalline samples of $Y_3Cu_9(OH)_{19}Cl_8$ obtained by a solid state reaction route [21], hence avoiding water in the preparation, disorder serves as chemical strain locally pinning the structure leading to the absence of structural transitions down to lowest temperatures [27]. External strain is, however, in comparison too weak to suppress LRO in this system [29]. Interestingly, such disordered powder samples of $Y_3Cu_9(OH)_{19}Cl_8$ without the structural anomaly showed a completely different μ SR spectrum and clear absence of LRO [21].

In addition to the chlorides, the sister compound series $YCu_3(OH)_6Br_2[Br_x(OH)_{1-x}]$ was also synthesized [37]. Here, the crystal structure determination proposed a mixture of the two end members similar to the Cl system, with partial occupancy of both Y sites, within and out of the kagomé layers, similar to crystals described in Ref. [30]. Variation of x has been reported [38–40] even reaching the composition $YCu_3(OH)_{6.5}Cl_{2.5}$ [37], which exceeds the endmember $x = 1/3$, i.e. $YCu_3(OH)_{19}Br_8$ [40]. Unfortunately, in most studies the crystal structures were not determined [41–43]. Recently, the Br system attracted particular attention due to signatures of a Dirac spin-liquid ground state [38, 39] based on a T^2 term in specific heat and a Dirac cone shaped excitation spectrum found in inelastic neutron scattering experiments [42]. Thermal transport studies revealed thermally acti-

vated phonon-spin scattering indicating a gapped magnetic excitation spectrum [41]. and 1/9 and 1/3 magnetization plateaus were found [43, 44]. In addition, quantum oscillations in torque measurements are observed for the first time in an insulator [44]. However, μ SR and NQR results revealed an inhomogeneous ground state with both fast and slow relaxing components [45]. Lately, by mixing Cl and Br the next level of complexity was reached [46–48].

Here, by using single crystal XRD, we report on investigations of the chemical disorder in $ZnCu_3(OH)_6Cl_2$ and, in particular, we compare in detail single crystals of the systems $YCu_3(OH)_6Cl_3$, $Y_3Cu_9(OH)_{19}Cl_8$, and $Y_3Cu_9(OH)_{19}Br_8$. By single crystal XRD we find for the Br systems the same superstructure as for the Cl variants leading to a distorted kagomé lattice, with the absence of mixed O/Br and Y site disorder. The physical properties of these crystals are similar to those reported in literature, with the distinction that now in the specific heat an anomaly at 15 K is observed which is field independent and likely similar to the 33 K anomaly in the Cl variant.

II. EXPERIMENTAL

A. Sample Preparation and Composition

Single crystals of $ZnCu_3(OH)_6Cl_2$ were grown similar to the recipe described in detail in Ref. 49 by placing a thick walled Pyrex glass ampoule ($\phi_{inner}=15$ mm, $\phi_{outer}=21$ mm, $l = 150$ mm) filled with 0.2g of CuO , 2g $ZnCl_2$, and 4 ml H_2O in an oven with temperature gradient of 150 to 180°C. The exact composition of the crystal used in XRD was determined by ICP-MS and gas extraction and found to be $Zn_{0.95(1)}Cu_{2.99(3)}O_{5.9(1)}H_{5.8(1)}Cl_2$.

Crystals of $YCu_3(OH)_6Cl_3$ and $Y_3Cu_9(OH)_{19}Cl_8$ were grown by two different routes following the descriptions provided in Refs. 19, 27, and 28: The first by a water-free hydroflux variant mixing 0.6g $LiOH$, 1.5g $BaCl_2$, 2g $Y(NO_3)_3 \cdot 6H_2O$, 1g $CuCl_2 \cdot 2H_2O$, and 0.6g $CuCl$ heated to 240°C for four days in a 23 ml teflon lined autoclave. The second by liquid phase transport of CuO in a YCl_3 - H_2O solution at elevated temperatures of 240°C at the hot end of similarly thick walled glass ampoules as used in the preparation of herbertsmithite.

Crystals of $Y_3Cu_9(OH)_{19}Br_8$ were synthesized following Ref. [37]. 0.6 g $Cu(NO_3)_2 \cdot 3H_2O$, 1.915 g $Y(NO_3)_3 \cdot 6H_2O$ and 1.785 g KBr (molar ratio $Cu : Y : Br = 1 : 2 : 6$) were mixed and 1 mL deionized water was added. Without further homogenization the mixture was transferred to a 23 mL teflon lined autoclave and heated to 230°C for 3 days. By repeating the synthesis several times we noticed that KBr is slowly creeping through the teflon liner and hence the process differs from the Cl case as crystallization is more a consequence of over-saturation and less of supercooling. Temperature variations confirmed this observation in the sense that higher temperatures led to a faster concentration change and different Br de-

ficient phases were found. We tested the variation of the composition, and the temperature profile and noticed that, similar to the Cl system, it is important to apply a temperature above 180°C as otherwise the parent compound $\text{Cu}_2(\text{OH})_3\text{Br}$ forms which undergoes a magnetic transition around 10 K [50]. Optimized synthesis conditions were obtained with 0.6 g $\text{Cu}(\text{NO}_3)_2 \cdot 3\text{H}_2\text{O}$ 1.9g $\text{Y}(\text{NO}_3)_3 \cdot 6\text{H}_2\text{O}$, 2.2 g KBr in 2.2 mL deionized water heated to 230°C for 2 days and subsequently quenched to room temperature.

B. Single Crystal XRD

XRD at room temperature was performed on single crystals of typical lateral sizes of 20 μm which had been broken off under high viscosity oil from larger items. The crystals were attached with vacuum grease on a loop made of Kapton foil (Micromounts, MiTeGen, Ithaca, NY). Diffraction data were collected with a SMART APEXI CCD X-ray diffractometer (Bruker AXS, Karlsruhe, Germany), using graphite-monochromated Mo-K_α radiation ($\lambda = 0.71073 \text{ \AA}$). The reflection intensities were integrated with the SAINT subprogram in the Bruker Suite software, a multi-scan absorption correction was applied using SADABS [51]. In case of $\text{Y}_3\text{Cu}_9(\text{OH})_{19}\text{Cl}_8$ and $\text{Y}_3\text{Cu}_9(\text{OH})_{19}\text{Br}_8$ the diffraction data show patterns of reverse/obverse twins (see Figures 3b and c), typical for rhombohedral symmetry. The data were corrected for this type of twinning applying multi-scan absorption correction with TWINABS [52]. All crystal structures were solved by direct methods and refined by full-matrix least-square fitting with the SHELXTL software package [51, 53].

C. Low temperature powder XRD

Low temperature powder XRD have been carried out using a Bruker D8 Venture with Cu K_α^1 radiation equipped with a closed-cycle He refrigerator. High statistic runs have been taken measuring in the range of 10 to 140° for 13 h in the range of 50-12 K.

D. Magnetization and Specific Heat

Magnetization measurements were performed on single crystals at temperatures $0.4 \leq T \leq 350 \text{ K}$ using a superconducting quantum interference device (MPMS-XL, Quantum Design) equipped with the He3 option. Specific-heat measurements were carried out, down to $T = 400 \text{ mK}$ in a Physical Properties Measurement System (PPMS, Quantum Design) similarly equipped with the He3 option.

TABLE I. Crystal structure data of the $\text{Zn}_{0.95(1)}\text{Cu}_{2.99(3)}\text{O}_{5.9(1)}\text{H}_{5.8(1)}\text{Cl}_2$ crystal refined assuming the space group $R\bar{3}m$ (no. 166) with $a = b = 6.8446(4) \text{ \AA}$, $c = 14.0935(13) \text{ \AA}$ and $R = 0.012$. In a separate table atom distances between the listed atom 1 and atom 2 are given,

atom	x	y	z	$U_{\text{iso}} (\text{\AA}^2)$	occ.	Wyck.
Zn1	0	0	0	0.01153(8)	0.6753(9)	3a
Cu1	0	0	0	0.01153(8)	0.3247(9)	3a
Cu2	0.5	0	0.5	0.0112(3)	0.8918(3)	9d
Zn2	0.5	0	0.5	0.017(3)	0.1082(3)	9d
Cl	0	0	0.30510(3)	0.01618(10)	1	6c
O	0.53930(7)	0.46070(7)	0.22816(5)	0.01392(14)	1	18h
H	0.477(3)	0.523(3)	0.2461(18)	0.039(8)	1	18h

atom 1	atom 2	distance (\AA)
Zn1/Cu1	O	2.1160(8)
Cu2/Zn2	O	1.9879(4)
Cu2/Zn2	Cl	2.7768(3)

III. RESULTS AND DISCUSSION

A. Herbertsmithite

Herbertsmithite is one of the best investigated QSL system with signatures of spinons seen in inelastic neutron scattering [4] and the clear absence of frozen spins in μSR [3]. As discussed above Zn:Cu site mixing can lead to structural and magnetic perturbations of the kagomé planes.

By single-crystal XRD we investigated an untwinned single crystal grown by the established recipe which according to chemical analysis had a composition of $\text{Zn}_{0.95(1)}\text{Cu}_{2.99(3)}\text{O}_{5.9(1)}\text{H}_{5.8(1)}\text{Cl}_2$.

Figure 1 shows zonal diffraction maps of this crystal and the refined crystal structure. A summary of the single crystal structure refinement is compiled in Table I.

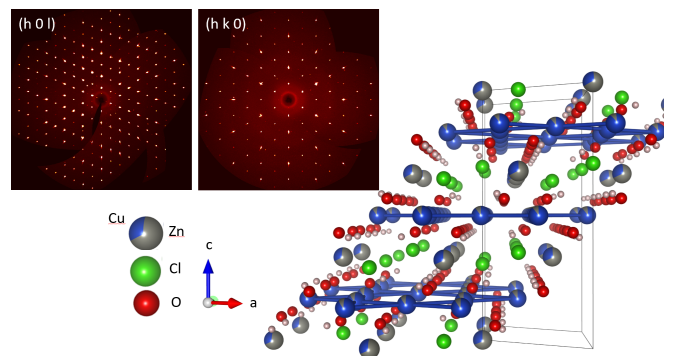


FIG. 1. Single crystal XRD zonal diffraction maps of the $\text{Zn}_{0.95(1)}\text{Cu}_{2.99(3)}\text{O}_{5.9(1)}\text{H}_{5.8(1)}\text{Cl}_2$ crystal and the resulting crystal structure viewed in a perspective mode from the single crystal data refinement ($R = 1.22$) revealing a substitution of 10.8% nonmagnetic Zn on the Cu sites.

The crystal structure of our crystal with composition $\text{Zn}_{0.95(1)}\text{Cu}_{2.99(3)}\text{O}_{5.9(1)}\text{H}_{5.8(1)}\text{Cl}_2$ was solved assuming the established space group $R\bar{3}m$ (no. 166) as given by

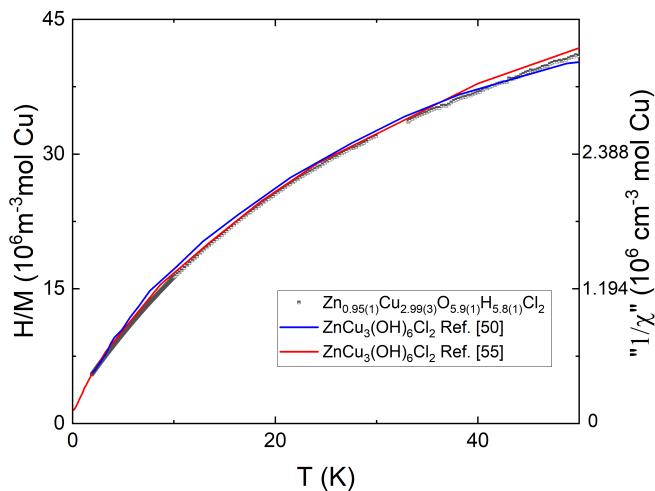


FIG. 2. Inverse M/H or as a function of temperature of our $x = 1$ herbertsmithite $\text{ZnCu}_3(\text{OH})_6\text{Cl}_2$ crystal compared to results of two other groups [49, 54] (reuse with permission). Note: The data by Bert *et al.* given in cgs units were converted to SI units and hence multiplied by 4π and the data by Han *et al.* by an additional correction factor of 1.18.

Braithwaite *et al.* and Shores *et al.*[55, 56]. First we refined the structure placing Zn on the expected interlayer Wyckoff site 3a and Cu on the kagomé site 9d reaching a satisfying refinement with $R = 0.0129$, $wR = 0.0315$, and a Goodness-of-fit, $\text{GOF} = 1.173$.

To consider possible Cu:Zn site mixing we allowed the Zn atoms to occupy the kagomé Cu site (Wyckoff sites 9d) and Cu atoms to substitute for the interlayer Zn atoms (Wyckoff site 3a). In view of the result of the chemical analysis we fixed the ratio of the substituted Zn:Cu atoms to 1 : 3. With this constraint we find 10.8% of nonmagnetic Zn ions in the kagomé planes. Refinement of the crystal structure allowing for site mixing improved the reliability factors to $R = 0.0122$, $wR = 0.0297$, and the Goodness-of-fit to $\text{GOF} = 1.115$. We note that the very similar xray scattering factors of Zn and Cu naturally make it difficult to locate the respective atom distribution with absolute certainty. However, our result gains some support from the powder neutron diffraction investigation by de Vries *et al.* who asserted very similar Zn:Cu mixing ratios [9]. We also emphasize that our investigated $\text{Zn}_{0.95(1)}\text{Cu}_{2.99(3)}\text{O}_{5.9(1)}\text{H}_{5.8(1)}\text{Cl}_2$ crystal showed no twinning which significantly alleviated and simplified the structure refinement reflected by the very low reliability factors.

The Zn atoms occupying sites within the kagomé layers dilute the magnetic system and induce random local distortion and strain since for Zn with a filled 3d electron shell the distortion of the O - Cl first anion coordination shell may be altered whereas the 32.4% Cu atoms on the 3a interlayer site tend to Jahn-Teller distort the coordinating oxygen octahedra a possibility already raised by Han *et al.*[12] As Norman *et al.* ana-

lyzed, the crystal structure of herbertsmithite is prone to symmetry lowering[14]. Local strain due to the Zn:Cu site mixing assists and stabilizes a higher symmetry, as it pins down the structure impeding distortions of the kagomé plane from magneto-phonon coupling, which happens here as the parent compound $\text{Cu}_2(\text{OH})_3\text{Cl}$ already above room temperature [32] moves from the trigonal herbertsmithite-type structure $R\bar{3}m$ to the monoclinic clinoatacamite-type structure $P2_1/n$ [32]. Even further symmetry lowering was found at low temperatures [31]. Via Zn substitution the high temperature $R\bar{3}$ is stabilized down to lowest temperatures in herbertsmithite.

The amount of free Cu spins can be estimated via the low temperature part in the magnetic susceptibility following Curie-Weiss law. We have measured several herbertsmithite crystals and found a remarkable reproducibility of the susceptibility at low temperatures. In Figure 2 we show the low temperature part of the inverse susceptibility or H/M in SI units of our crystal compared to literature data taken from Refs. 49 and 54. The data by Han *et al.* were multiplied by a factor 1.18, as there was an apparent scaling difference likely from small errors in the sample mass determination. The good congruence of the magnetic susceptibilities from different sources and the good agreement of our XRD single crystal refinement results with the neutron power diffraction findings points to an equilibrium Cu-Zn site mixing level throughout herbertsmithite.

B. $\text{YCu}_3(\text{OH})_6\text{Cl}_3$ and $\text{Y}_3\text{Cu}_9(\text{OH})_{19}\text{X}_8$ ($\text{X}=\text{Cl}, \text{Br}$)

The example of herbertsmithite raises the question, as to the role of disorder in the $\text{YCu}_3(\text{OH})_6\text{Cl}_3$ and $\text{Y}_3\text{Cu}_9(\text{OH})_{19}\text{X}_8$ ($\text{X}=\text{Cl}, \text{Br}$) kagomé systems. We therefore investigated in detail their crystal structure by single crystal XRD. To start with we initially performed single crystal XRD on crystals of $\text{YCu}_3(\text{OH})_6\text{Cl}_3$ and subsequently on $\text{Y}_3\text{Cu}_9(\text{OH})_{19}\text{Cl}_8$. Our structure analysis proves the space group $P\bar{3}m1$ (no. 164) for $\text{YCu}_3(\text{OH})_6\text{Cl}_3$, as reported before[19]. In addition, weak superstructure Bragg reflections (see Fig. 3b) are seen for $\text{Y}_3\text{Cu}_9(\text{OH})_{19}\text{Cl}_8$ which violate the selection rules for the higher symmetry space group $P\bar{3}m1$, but can be readily explained by performing a refinement in space group $R\bar{3}$ (no. 148) with a tripled unit cell. [25] Notably, $R\bar{3}$ is a structural subgroup of $P\bar{3}m1$.

Next, we performed single crystal XRD on a crystal with nominal composition $\text{YCu}_3(\text{OH})_6\text{Br}_2[\text{Br}_x(\text{OH})_{1-x}]$. Zonal diffraction maps and the crystal structure are depicted in Figure 3 c). Again clear superstructure Bragg reflections are visible, similar to the Cl homologue, indicating a symmetry reduction from $P\bar{3}m1$. A structure description in space group $R\bar{3}$ (no. 148) proved successful with the refinement results summarized in Table II. The apparent very similar crystal structure refinement results of the Cl and Br crystals suggests the composition of the

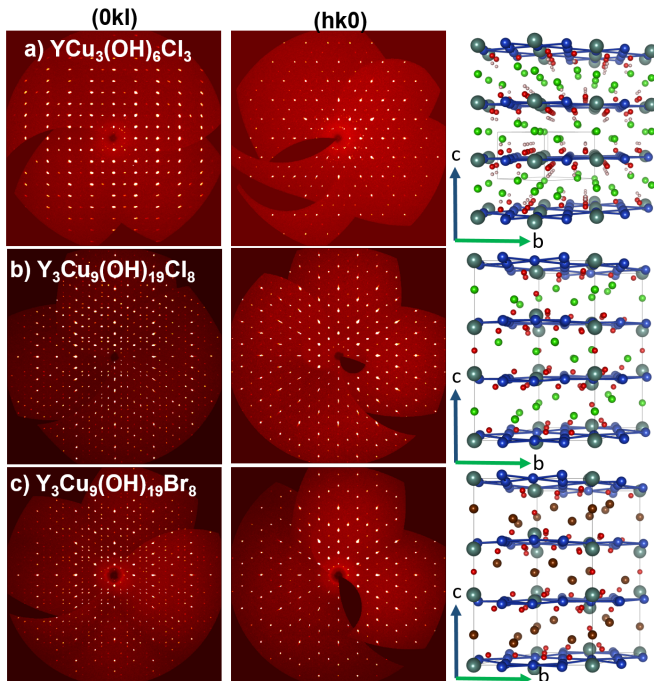


FIG. 3. Zonal XRD maps of single crystals of a) $\text{YCu}_3(\text{OH})_6\text{Cl}_3$ ($R=0.0358$, $GOF=1.018$), b) $\text{Y}_3\text{Cu}_9(\text{OH})_{19}\text{Cl}_8$ ($R=0.0339$, $GOF=1.028$), and c) $\text{Y}_3\text{Cu}_9(\text{OH})_{19}\text{Br}_8$ ($R=0.038$, $GOF=1.04$) as well as their crystal structure in a perspective view projected along a^* as obtained from our single crystal structure refinements. Cu atoms are displayed in blue, Y atoms in metallic grey, and Cl and Br atoms in green and brown, respectively

Br homologue accordingly as $\text{Y}_3\text{Cu}_9(\text{OH})_{19}\text{Br}_8$.

Notably our synthesis of the $\text{Y}_3\text{Cu}_9(\text{OH})_{19}\text{Br}_8$ crystals did not differ essentially from that of Ref. 37. However, we found in our growth batches both chemically disordered (typically optically intransparent) and chemically ordered Y-Kapellsite-type crystals. This finding suggests that for the published crystal structure those Y atoms which moved out of the kagomé plane will locally distort the kagomé lattice and hence release frustration. We conclude that there is simply a mixture of domains with distorted and undistorted local structures, averaging to the partially occupied scenario.

The level of distortion of the kagomé lattice is clearly reflected by the lowest Cu-Cu-Cu angles. For $\text{Y}_3\text{Cu}_9(\text{OH})_{19}\text{Cl}_8$ the Cu-Cu-Cu angle amounts to $176.12(3)^\circ$. Notably, this angle is further lowered for $\text{Y}_3\text{Cu}_9(\text{OH})_{19}\text{Br}_8$ to $174.71(3)^\circ$.

The exchange interactions were calculated for the Cl variant and a rather low J' was found for the shortest Cu-Cu bond, Cu1 - Cu2 of $3.2582(6)$ Å [26]. The corresponding Cu1 - O - Cu2 bond angle amounts to $110.93(13)^\circ$, whereas the elongated Cu2 - O - Cu1 and Cu1 - O - Cu1 bonds enclose an angle of $\approx 118^\circ$. As can be expected for the larger anion Br^- , we find a subtle elongation of this short Cu1 - Cu2 bond to $3.2640(4)$ Å for the Br homologue, while the bonding angle with $110.63(9)^\circ$ remains

TABLE II. Single crystal XRD results (atom fractional coordinates, atom displacement parameters U_{iso} , occupancies) obtained for a crystal with composition $\text{Y}_3\text{Cu}_9(\text{OH})_{19}\text{Br}_8$. The refinement was carried out assuming the space group $R\bar{3}$ (no. 148) and the lattice parameters converged to $a = b = 11.5945(5)$ Å, $c = 18.2302(11)$ Å. In a separate table the atom distances between the listed atom 1 and atom 2 are given,

Site	x	y	z	U_{iso} (Å ²)	occ.
Br1	0	0	0.83774(2)	0.01823(9)	1
Br2	0.33194(2)	0.00211(2)	0.78497(2)	0.01895(7)	1
Y1	0	0	0.62289(2)	0.01134(8)	1
Y2	0	0	0	0.01351(10)	1
Cu1	0.17073(3)	-0.15827(3)	0.66160(2)	0.01271(7)	1
Cu2	0.5	0	0	0.01271(8)	1
O1	0	0	0.5	0.0404(15)	1
O2	0.00241(19)	-0.17029(16)	0.69711(10)	0.0129(3)	1
O3	0.3427(2)	-0.13493(18)	0.62560(10)	0.0125(3)	1
O4	0.20379(17)	0.00614(19)	0.61068(9)	0.0124(3)	1

	atom 1	atom 2	distance (Å)
	Cu1	O2	2.0047(18)
	Cu1	O4	1.9916(18)
	Cu1	Br2	2.8741(3)
	Cu2	O2	1.9938(18)
	Cu2	O3	1.981(2)
	Cu2	O4	1.9778(18)
	Cu2	Br2	2.8974(4)

nearly unchanged. Interestingly, the Cu2 - O - Cu1 bond is strongly shortened and encloses an angle of $113.9(7)^\circ$, whereas the longest Cu2 - O - Cu2 bond remains relatively large with a bonding angle of $116.4(7)^\circ$. As the antiferromagnetic superexchange is strongest close to 180° this hints toward a movement in direction of the QSL phase in the phase diagram given by Hering *et al.* [26].

Naturally, to understand the physical properties of a system, it is best to investigate the chemically 'clean' phase-pure scenario. Hence, we characterized our $\text{Y}_3\text{Cu}_9(\text{OH})_{19}\text{Br}_8$ crystals and measured their specific heat in the range temperature range from 0.4 to 40 K depicted in Figure 4 a). Quite similar to literature and the Cl case we find a field-dependent maximum at around 2.25 K indicating a magnetic transition also confirmed by spin wave measurements and multi-magnon excitations [27, 28]. However, unlike literature, we observe a relatively sharp (in comparison to the magnetic transition in $\text{YCu}_3(\text{OH})_6\text{Cl}_3$) field-independent peak at 15 K. For $\text{Y}_3\text{Cu}_9(\text{OH})_{19}\text{Cl}_8$ there is only the 33 K anomaly in specific heat [27] (not shown here), while in thermal expansion and NMR a clear transition is also seen at the same temperature of 15 K [27]. In summary, this anomaly at 15 K likely originates from structural origin. The T^2 slope of the specific heat in the narrow temperature range of $0 < T < 0.75$ K below the 2.5 K peak was attributed to a Dirac-like T^2 scenario.39 and 41 However, such slope is equally well described by spin waves excitations and does not differ essentially from the behavior of the Cl homologue in this temperature range.

To investigate the low-temperature transition around

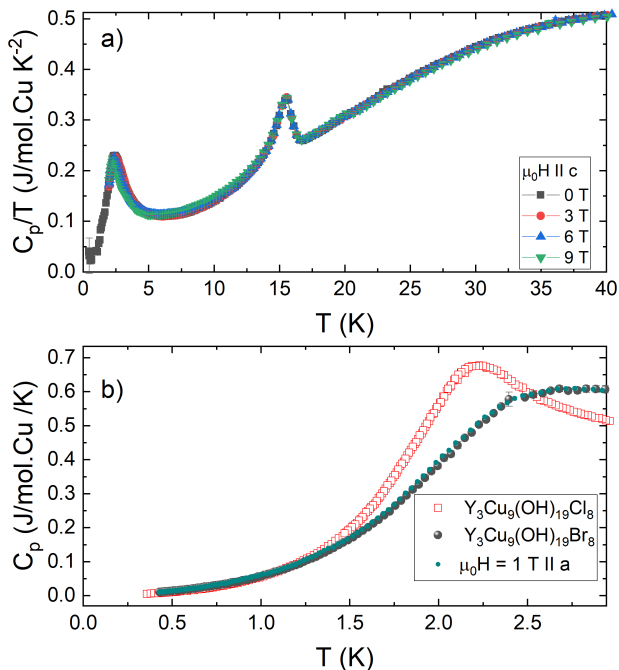


FIG. 4. a) Specific heat versus temperature of nine co-aligned $\text{Y}_3\text{Cu}_9(\text{OH})_{19}\text{Br}_8$ single crystals with a total mass of 1.66 mg. b) Low temperature specific heat part of $\text{Y}_3\text{Cu}_9(\text{OH})_{19}\text{Br}_8$ compared to our data of $\text{Y}_3\text{Cu}_9(\text{OH})_{19}\text{Cl}_8$ [25].

15 K we have carried out low-temperature powder XRD (PXR) from 300 to 12 K, in a Bragg-Brentano setup, where the powder was first only spread on the sample holder with ethanol. At the structural transition due to a sudden volume change the sample jumped and we saw a zero shift looking like a cell contraction. Notably, this is well in line with thermal expansion measurements on the Cl counterpart [27]. We then remeasured the sample mixed with ApiezonN grease. A selection of the PXR data is shown in Figure 5 where no sudden symmetry reduction is observed as no peak splittings, nor sudden changes of the peak positions are visible. The transition certainly is of structural origin as besides our observation of sample jumping at exactly 18 K, a tiny anomaly in the crystal volume from Rietveld refinements and a deviation of the typical L-shape of the Volume change (see Figure 5 d), we find a peak splitting in Br-NMR [57]. Hence, we have confirmed a similar subtle structural transition in the Br counterpart as in the Cl, which cannot be captured by simple PXR, which likely stems from subtle hydrogen movements influenced by the magnetism. It is reasonable to assume that the system releases its magnetic frustration via a subtle structural distortion, notably the supercell and Cu distortion of two sites anyways is large enough to place us in the LRO scenario of the magnetic phase diagram [26] and hence the system is likely finally resulting in LRO around 2 K very similar to its Cl counterpart [27]. In contrast the site disordered system shows no 15 K transition in specific heat [38, 39].

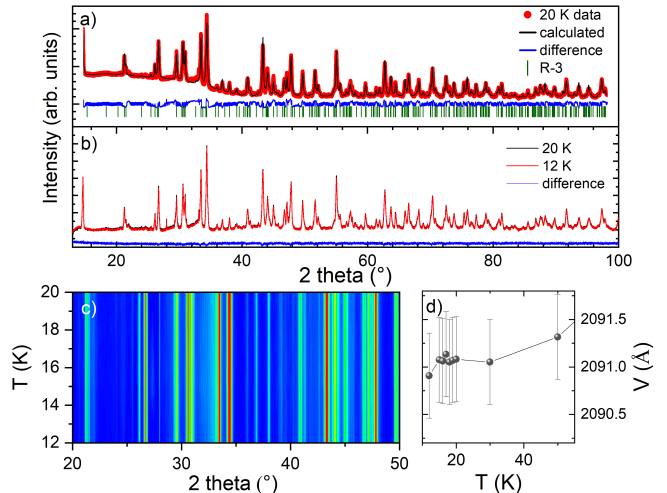


FIG. 5. (a) 12 K PXR pattern (red) as well as the Rietveld profile refinement assuming the $R\bar{3}$ structure. (b) 20 K (black) and 12 K (red) PXR pattern and the difference between them (blue). (c) Contour plots of a selected range of the PXR data from 20-15 K revealing no major structural changes captured by PXR. (d) Volume extracted from Rietveld refinements versus temperature.

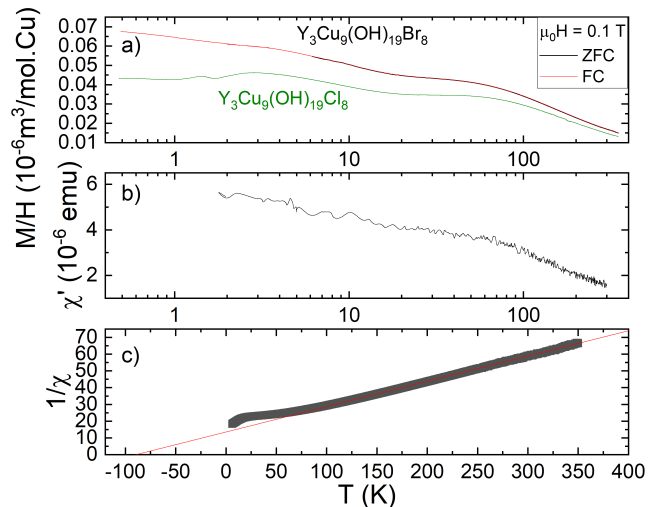


FIG. 6. a) Magnetization versus temperature on a semi-log plot of a collection of crystals of $\text{Y}_3\text{Cu}_9(\text{OH})_{19}\text{Br}_8$ with a mass of 63 mg (zero field cooled: black, field cooled: red) compared to our data of $\text{Y}_3\text{Cu}_9(\text{OH})_{19}\text{Cl}_8$ (green) [28]. b) AC susceptibility versus temperature on a semi-log plot. c) Inverse magnetization versus temperature fitted to a Curie-Weiss law.

As shown in Figure 6 a) the magnetization versus temperature of $\text{Y}_3\text{Cu}_9(\text{OH})_{19}\text{Br}_8$ looks remarkably similar to that of the Cl homologue except for the slope below 2.5 K, where the Cl phase shows several maxima and the Br phase exhibits a continuous increase, mainly from impurity spins. AC susceptibility measurements (see Figure 6 b) only indicate a subtle increase on lowering the temperature, while a clear slope change is visible at around

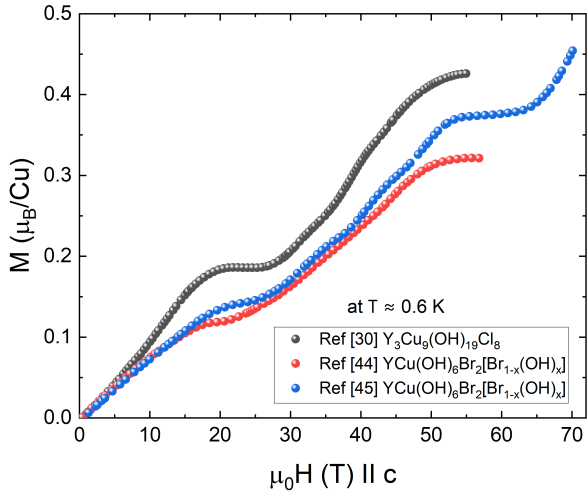


FIG. 7. Reproduction from literature of the magnetization versus magnetic field of our data on $\text{Y}_3\text{Cu}_9(\text{OH})_{19}\text{Cl}_8$ [28] and data on $\text{YCu}_3(\text{OH})_6\text{Br}_2[\text{Br}_x(\text{OH})_{1-x}]$ [43, 44] (reuse with permission) measured at ~ 0.6 K for fields applied perpendicular to the kagomé plane.

15 K both in DC and AC, similar as for the Cl system. A Curie-Weiss fit of the inverse susceptibility shown in Figure 6 c) yields a Curie-Weiss temperature of -90 K and a slope of 0.153 corresponding to an effective moment of $2 \mu_B$, consistent with typical effective moments of Cu^{2+} systems. All these findings are in good agreement with published results describing the disordered $\text{YCu}_3(\text{OH})_6\text{Br}_2[\text{Br}_x(\text{OH})_{1-x}]$ phase [37, 38] and hint towards uniform physical properties rather insensitive to the disorder.

Finally, in Figure 7 we compare the magnetizations as a function of the magnetic field collected at ~ 0.6 K of the two compounds $\text{Y}_3\text{Cu}_9(\text{OH})_{19}\text{Cl}_8$ [28] and $\text{YCu}_3(\text{OH})_6\text{Br}_2[\text{Br}_x(\text{OH})_{1-x}]$ as reported in literature [28, 43, 44]. Both compounds show magnetization plateaus at similar fields with the difference of the saturation value possibly originating from background signal, sample mass uncertainties and/or alignment issues as there is a sizable anisotropy. This already becomes apparent when comparing the two literature values of the same Br sample. Assuming that there are no such errors, $\text{Y}_3\text{Cu}_9(\text{OH})_{19}\text{Cl}_8$ displays a $1/6$ magnetization plateau and $\text{YCu}_3(\text{OH})_6\text{Br}_2[\text{Br}_x(\text{OH})_{1-x}]$ a $1/9$ plateau. However, given the structural similarities, similar physical properties can be expected. As we are in the same region of exchange interactions in the phase diagram proposed by Hering *et al.* [26] we suggest that we observe similar magnetization plateaus in the two compounds.

In addition, a comparison of the INS spectra of the two compounds $\text{Y}_3\text{Cu}_9(\text{OH})_{19}\text{Cl}_8$ collected at 1.5 K (Ref. 27) and $\text{YCu}_3(\text{OH})_6\text{Br}_2[\text{Br}_x(\text{OH})_{1-x}]$ collected at 0.3 K (Ref. 42), is very suggestive that the same ground state is realized in both systems independent of disorder. The randomness induced by disorder simply increases the al-

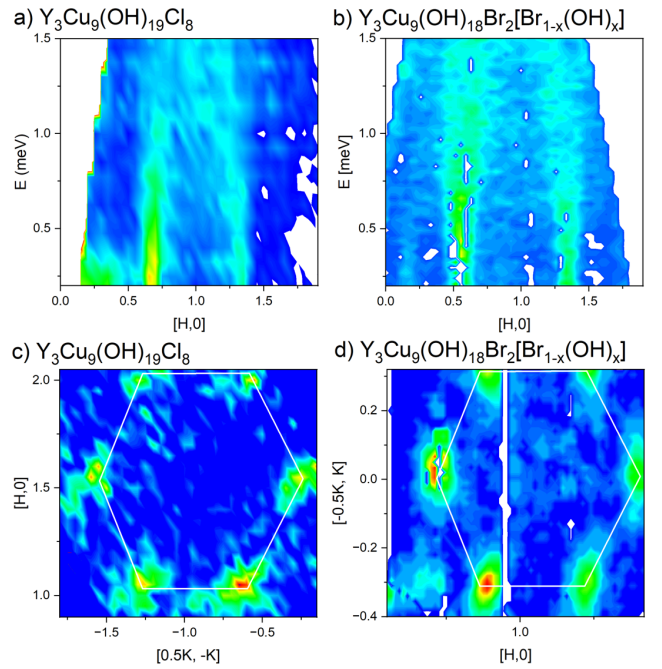


FIG. 8. Reproduction from literature of the inelastic neutron scattering data of a,c) $\text{Y}_3\text{Cu}_9(\text{OH})_{19}\text{Cl}_8$ at 1.5 K [27] and b,d) $\text{YCu}_3(\text{OH})_6\text{Br}_2[\text{Br}_x(\text{OH})_{1-x}]$ at 0.3 K [42] (note that the intensities are in arbitrary units. In a,c) energy integrated plots are shown around 0.2 and 0.4 meV and in b,d) Intensity contour plots of the INS results are given as a function of E and Q along the $[\text{H},0]$ direction.

ready quite broad distribution of J' that exists in the Cl homologue as described by Chatterjee *et al.* [27]. The scenario of randomness smearing out spin waves was well documented for $\text{Sr}_2\text{CuTe}_{1-x}\text{W}_x\text{O}_6$ [58]. Via a continuous increase of randomness by substitution of Te by W it was demonstrated that the bond randomness, rather than the residual frustration, drives the physics of the system. The corresponding INS spectra simply smear out, while retaining their main features. However, we see a clear difference for the disorder free system as we find a structural transition at low temperatures, which is absent in the disordered crystals. Hence it is possible, that a spin liquid phase might be formed similar as in herbertsmithite.

IV. SUMMARY

In summary, we conclude that disorder clearly suppresses structural anomalies such as the 8 K transition of clinoatacamite in the Zn variant herbertsmithite, the 15 K transition in $\text{Y}_3\text{Cu}_9(\text{OH})_{19}\text{Br}_8$ or the 33 K transition in $\text{Y}_3\text{Cu}_9(\text{OH})_{19}\text{Cl}_8$. These structural transitions slightly distort the kagomé and release frustration leading to magnetic LRO. In the disordered systems signatures of LRO are less clear, as domains of distorted and undistorted kagomé layers co-exist preventing long spin

waves to establish. As disorder appears to be a common feature in these systems it remains to be studied in more detail to what extent bond randomness is an essential ingredient for the physics of all existing QSL systems. The chemo - structural disorder in the kagomé spin $S = 1/2$ systems $\text{ZnCu}_3(\text{OH})_6\text{Cl}_2$, found in a similar magnitude for independent samples and by different groups, leads to a substantial randomness with $\sim 11\%$ nonmagnetic spins in the kagomé plane. Similarly in

$\text{YCu}_3(\text{OH})_6\text{Br}_2[\text{Br}_x(\text{OH})_{1-x}]$ due to the mixture of two structural variants with $x = 0$ and $x = 1/3$. randomness is present for intermediate substitutions. The magnetic properties of our $x = 1/3$ crystals resemble those of the Cl compound with a low-temperature structural transition emerging from strong magneto-elastic coupling as a release of frustration. The very close similarity of their physical properties of the two sister compounds suggests a $(1/3, 1/3)$ ground-state possibly even for the disordered $\text{YCu}_3(\text{OH})_6\text{Br}_2[\text{Br}_x(\text{OH})_{1-x}]$ phases.

-
- [1] L. Balents, Spin liquids in frustrated magnets, *Nature* **464**, 199 (2010).
- [2] J. R. Chamorro, T. M. McQueen, and T. T. Tran, Chemistry of Quantum Spin Liquids, *Chemical Reviews* **121**, 2898 (2020).
- [3] P. Mendels, F. Bert, M. A. de Vries, A. Olariu, A. Harrison, F. Duc, J. C. Trombe, J. S. Lord, A. Amato, and C. Baines, Quantum Magnetism in the Paratacamite Family: Towards an Ideal Kagomé Lattice, *Phys. Rev. Lett.* **98**, 077204 (2007).
- [4] T.-H. Han, J. S. Helton, S. Chu, D. G. Nocera, J. A. Rodriguez-Rivera, C. Broholm, and Y. S. Lee, Fractionalized excitations in the spin-liquid state of a kagome-lattice antiferromagnet, *Nature* **492**, 406 (2012).
- [5] K. Tustain, B. Ward-O'Brien, F. Bert, T. Han, H. Luetkens, T. Lancaster, B. M. Huddart, P. J. Baker, and L. Clark, From magnetic order to quantum disorder in the Zn-barlowite series of $S = 1/2$ kagomé antiferromagnets, *npj Quantum Materials* **5**, 74 (2020).
- [6] Y. Fu, M.-L. Lin, L. Wang, Q. Liu, L. Huang, W. Jiang, Z. Hao, C. Liu, H. Zhang, X. Shi, J. Zhang, J. Dai, D. Yu, F. Ye, P. A. Lee, P.-H. Tan, and J.-W. Mei, Dynamic fingerprint of fractionalized excitations in single-crystalline $\text{Cu}_3\text{Zn}(\text{OH})_6\text{FBr}$, *Nature Communications* **2021 12:1**, 12, 1 (2021).
- [7] T. Imai, E. A. Nytko, B. M. Bartlett, M. P. Shores, and D. G. Nocera, $\text{Cu}^{63}, \text{Cl}^{35}$, and H^1 NMR in the $S=1/2$ Kagome Lattice $\text{ZnCu}_3(\text{OH})_6\text{Cl}_2$, *Physical Review Letters* **100**, 077203 (2008).
- [8] M. J. Rozenberg and R. Chitra, Disorder effects in the quantum kagome antiferromagnet $\text{ZnCu}_3(\text{OH})_6\text{Cl}_2$, *Physical Review B* **78**, 132406 (2008).
- [9] M. A. de Vries, K. V. Kamenev, W. A. Kockelmann, J. Sanchez-Benitez, and A. Harrison, Magnetic ground state of an experimental $s = 1/2$ kagome antiferromagnet, *Phys. Rev. Lett.* **100**, 157205 (2008).
- [10] M. A. deVries and A. Harrison, Model's reputation restored, *Nature* **468**, 908 (2010).
- [11] D. E. Freedman, T. H. Han, A. Prodi, P. Müller, Q.-Z. Huang, Y.-S. Chen, S. M. Webb, Y. S. Lee, T. M. McQueen, and D. G. Nocera, Site Specific X-ray Anomalous Dispersion of the Geometrically Frustrated Kagomé Magnet, Herbertsmithite, $\text{ZnCu}_3(\text{OH})_6\text{Cl}_2$, *Journal of the American Chemical Society* **132**, 16185 (2010).
- [12] T.-H. Han, M. R. Norman, J.-J. Wen, J. A. Rodriguez-Rivera, J. S. Helton, C. Broholm, and Y. S. Lee, Correlated impurities and intrinsic spin-liquid physics in the kagome material herbertsmithite, *Physical Review B* **94**, 060409 (2016).
- [13] A. Zorko, M. Herak, M. Gomilšek, J. van Tol, M. Velázquez, P. Khuntia, F. Bert, and P. Mendels, Symmetry reduction in the quantum kagome antiferromagnet herbertsmithite, *Phys. Rev. Lett.* **118**, 017202 (2017).
- [14] M. R. Norman, N. J. Laurita, and D. Hsieh, Valence bond phases of herbertsmithite and related copper kagome materials, *Phys. Rev. Res.* **2**, 013055 (2020).
- [15] M. Fu, T. Imai, T.-H. Han, and Y. S. Lee, Evidence for a gapped spin-liquid ground state in a kagome heisenberg antiferromagnet, *Science* **350**, 655 (2015).
- [16] D. Wulferding, P. Lemmens, P. Scheib, J. Röder, P. Mendels, S. Chu, T. Han, and Y. S. Lee, Interplay of thermal and quantum spin fluctuations in the kagome lattice compound herbertsmithite, *Physical Review B* **82**, 144412 (2010).
- [17] P. Khuntia, M. Velazquez, Q. Barthélemy, F. Bert, E. Kermarrec, A. Legros, B. Bernu, L. Messio, A. Zorko, and P. Mendels, Gapless ground state in the archetypal quantum kagome antiferromagnet $\text{ZnCu}_3(\text{OH})_6\text{Cl}_2$, *Nature Physics* **16**, 469 (2020).
- [18] P. Puphal, K. M. Zoch, J. Désor, M. Bolte, and C. Krellner, Kagome quantum spin systems in the atacamite family, *Physical Review Materials* **2**, 063402 (2018).
- [19] W. Sun, Y.-X. Huang, S. Nokhrin, Y. Pan, and J.-X. Mi, Perfect Kagomé lattices in $\text{YCu}_3(\text{OH})_6\text{Cl}_3$: a new candidate for the quantum spin liquid state, *Journal of Materials Chemistry C* **4**, 8772 (2016).
- [20] Y. Fu, L. Huang, X. Zhou, J. Chen, X. Zhang, P. Chen, S. Wang, C. Liu, D. Yu, H.-F. Li, L. Wang, and J.-W. Mei, $\text{LnCu}_3(\text{OH})_6\text{Cl}_2$ ($\text{Ln} = \text{Gd}, \text{Tb}, \text{Dy}$): Heavy lanthanides on spin-1/2 kagome magnets, *Chinese Physics B* **30**, 100601 (2021).
- [21] Q. Barthélemy, P. Puphal, K. M. Zoch, C. Krellner, H. Luetkens, C. Baines, D. Sheptyakov, E. Kermarrec, P. Mendels, and F. Bert, Local study of the insulating quantum kagome antiferromagnets $\text{YCu}_3(\text{OH})_6\text{O}_x\text{Cl}_{3-x}$ ($x=0, 1/3$), *Physical Review Materials* **3**, 074401 (2019).
- [22] A. Zorko, M. Pregelj, M. Gomilšek, M. Klanjšek, O. Zaharko, W. Sun, and J.-X. Mi, Negative-vector-chirality 120° spin structure in the defect- and distortion-free quantum kagome antiferromagnet $\text{YCu}_3(\text{OH})_6\text{Cl}_3$, *Physical Review B* **100**, 144420 (2019).
- [23] A. Zorko, M. Pregelj, M. Klanjšek, M. Gomilšek, Z. Jagličić, J. S. Lord, J. A. T. Verezhak, T. Shang, W. Sun, and J.-X. Mi, Coexistence of magnetic order and persistent spin dynamics in a quantum kagome antiferromagnet with no intersite mixing, *Physical Review B* **99**, 214441 (2019).

- [24] P. Prelovsek, M. Gomilšek, T. Arh, and A. Zorko, Dynamical spin correlations of the kagome antiferromagnet, *Physical Review B* **103**, 014431 (2021).
- [25] P. Puphal, M. Bolte, D. Sheptyakov, A. Pustogow, K. Kliemt, M. Dressel, M. Baenitz, and C. Krellner, Strong magnetic frustration in $Y_3Cu_9(OH)_{19}Cl_8$: a distorted kagome antiferromagnet, *Journal of Materials Chemistry C* **5**, 2629 (2017).
- [26] M. Hering, F. Ferrari, A. Razpopov, I. I. Mazin, R. Valentí, H. O. Jeschke, and J. Reuther, Phase diagram of a distorted kagome antiferromagnet and application to Y-kapellasite, *npj Computational Materials* **8**, 1 (2022).
- [27] D. Chatterjee, P. Puphal, Q. Barthélemy, J. Willwater, S. Süllow, C. Baines, S. Petit, E. Ressouche, J. Ollivier, K. M. Zoch, C. Krellner, M. Parzer, A. Riss, F. Garmroudi, A. Pustogow, P. Mendels, E. Kermarrec, and F. Bert, From spin liquid to magnetic ordering in the anisotropic kagome Y-kapellasite $Y_3Cu_9(OH)_{19}Cl_8$: A single-crystal study, *Physical Review B* **107**, 125156 (2023).
- [28] T. Biesner, S. Roh, A. Razpopov, J. Willwater, S. Süllow, Y. Li, K. M. Zoch, M. Medarde, J. Nuss, D. Gorbunov, Y. Skourski, A. Pustogow, S. E. Brown, C. Krellner, R. Valentí, P. Puphal, and M. Dressel, Multi-Center Magnon Excitations Open the Entire Brillouin Zone to Terahertz Magnetometry of Quantum Magnets, *Advanced Quantum Technologies* **5**, 2200023 (2022).
- [29] J. Wang, M. Spitaler, Y.-S. Su, K. Zoch, C. Krellner, P. Puphal, S. Brown, and A. Pustogow, Controlled frustration release on the kagome lattice by uniaxial-strain tuning, *Physical Review Letters* **131**, 256501 (2023).
- [30] W. Sun, T. Arh, M. Gomilšek, P. Koželj, S. Vrtnik, M. Herak, J.-X. Mi, and A. Zorko, Magnetic ordering of the distorted kagome antiferromagnet $Y_3Cu_9(OH)_{18}[Cl_8(OH)]$ prepared via optimal synthesis, *Physical Review Materials* **5**, 064401 (2021).
- [31] X. G. Zheng, M. Fujihala, S. Kitajima, M. Maki, K. Kato, M. Takata, and C. N. Xu, Strong magnetic-dielectric-lattice coupling in transition metal hydroxyhalides and ferroelectric response in rhombohedral $Co_2(OD)_{3x}(x=cl, br)$, *Physical Review B* **87**, 174102 (2013).
- [32] T. Malcherek, B. Mihailova, and M. D. Welch, Structural phase transitions of clinoatacamite and the dynamic jahn-teller effect, *Phys. Chem. Miner.* **44**, 307 (2017).
- [33] A. Henderson, L. Dong, S. Biswas, H. I. Revell, Y. Xin, R. Valenti, J. A. Schlueter, and T. Siegrist, Order-disorder transition in the $S = \frac{1}{2}$ kagome antiferromagnets claringbullite and barlowite, *Chemical Communications* **55**, 11587 (2019).
- [34] H. Ishikawa, M. Yoshida, K. Nawa, M. Jeong, S. Krämer, M. Horvatić, C. Berthier, M. Takigawa, M. Akaki, A. Miyake, M. Tokunaga, K. Kindo, J. Yamaura, Y. Okamoto, and Z. Hiroi, One-Third Magnetization Plateau with a Preceding Novel Phase in Volborthite, *Physical Review Letters* **114**, 227202 (2015).
- [35] D. Boldrin, K. Knight, and A. S. Wills, Orbital frustration in the $S = 1/2$ kagome magnet vesignieite, $BaCu_3V_2O_8(OD)_2$ (2016), [arXiv:1610.01436 \[cond-mat.mtrl-sci\]](https://arxiv.org/abs/1610.01436).
- [36] P. Dolezal, T. Biesner, Y. Li, R. Mathew Roy, S. Roh, R. Valentí, M. Dressel, P. Puphal, and A. Pustogow, Lattice dynamics of the frustrated kagome compound y-kapellasite, to be published (2024).
- [37] X.-H. Chen, Y.-X. Huang, Y. Pan, and J.-X. Mi, Quantum spin liquid candidate $YCu_3(OH)_6Br_2[Br(OH)_{1-x}]$ ($x \approx 0.51$): With an almost perfect kagomé layer, *Journal of Magnetism and Magnetic Materials* **512**, 167066 (2020).
- [38] Z. Zeng, X. Ma, S. Wu, H.-F. Li, Z. Tao, X. Lu, X.-h. Chen, J.-X. Mi, S.-J. Song, G.-H. Cao, G. Che, K. Li, G. Li, H. Luo, Z. Y. Meng, and S. Li, Possible Dirac quantum spin liquid in the kagome quantum antiferromagnet $YCu_3(OH)_6Br_2[Br_x(OH)_{1-x}]$, *Phys. Rev. B* **105**, L121109 (2022).
- [39] J. Liu, L. Yuan, X. Li, B. Li, K. Zhao, H. Liao, and Y. Li, Gapless spin liquid behavior in a kagome Heisenberg antiferromagnet with randomly distributed hexagons of alternate bonds, *Physical Review B* **105**, 024418 (2022).
- [40] F. Lu, L. Yuan, J. Zhang, B. Li, Y. Luo, and Y. Li, The observation of quantum fluctuations in a kagome heisenberg antiferromagnet, *Communications Physics* **5**, 10.1038/s42005-022-01053-4 (2022).
- [41] X. Hong, M. Behnami, L. Yuan, B. Li, W. Brenig, B. Büchner, Y. Li, and C. Hess, Heat transport of the kagome Heisenberg quantum spin liquid candidate $YCu_3(OH)_{6.5}Br_{2.5}$: Localized magnetic excitations and a putative spin gap, *Physical Review B* **106**, 1220406 (2022).
- [42] Z. Zeng, C. Zhou, H. Zhou, L. Han, R. Chi, K. Li, M. Kofu, K. Nakajima, Y. Wei, W. Zhang, D. G. Mazzone, Z. Y. Meng, and S. Li, Spectral evidence for dirac spinons in a kagome lattice antiferromagnet, *Nature Physics* **20**, 1097 (2024).
- [43] S. Suetsugu, T. Asaba, Y. Kasahara, Y. Kohsaka, K. Tokusaka, B. Li, Y. Zhao, Y. Li, M. Tokunaga, and Y. Matsuda, Emergent spin-gapped magnetization plateaus in a spin-1/2 perfect kagome antiferromagnet, *Physical Review Letters* **132**, 226701 (2024).
- [44] G. Zheng, Y. Zhu, K.-W. Chen, B. Kang, D. Zhang, K. Jenkins, A. Chan, Z. Zeng, A. Xu, O. A. Valenzuela, J. Blawat, J. Singleton, P. A. Lee, S. Li, and L. Li, *Unconventional magnetic oscillations in kagome mott insulators* (2023).
- [45] C. Lee, W. Lee, S. Lee, T. Yamanaka, S. Jeon, J. Khatua, H. Nojiri, and K.-Y. Choi, Dirac spinons intermingled with singlet states in the random kagome antiferromagnet $YCu_3(OD)_{6+x}Br_{3-x}$ ($x=0.5$), *Physical Review B* **110**, 064418 (2024).
- [46] S. Li, Y. Cui, Z. Zeng, Y. Wang, Z. Hu, J. Liu, C. Li, X. Xu, Y. Chen, Z. Liu, S. Li, and W. Yu, NMR evidence of spinon localization in the kagome antiferromagnet $YCu_3(OH)_6Br_2[Br_x(OH)_{1-x}]$, *Physical Review B* **109**, 104403 (2024).
- [47] B. S. Shivaram, J. Prestigiacomo, A. Xu, Z. Zeng, T. D. Ford, I. Kimchi, S. Li, and P. A. Lee, *Non-analytic magnetic response and intrinsic ferromagnetic clusters in a dirac spin liquid candidate* (2024).
- [48] A. Xu, Q. Shen, B. Liu, Z. Zeng, L. Han, L. Yan, J. Luo, J. Yang, R. Zhou, and S. Li, Magnetic ground states in the kagome system $YCu_3(OH)_6[(Cl_xBr_{1-x})_{1-y}(OH)_y]$, *Physical Review B* **110**, 085146 (2024).
- [49] T. H. Han, J. S. Helton, S. Chu, A. Prodi, D. K. Singh, C. Mazzoli, P. Müller, D. G. Nocera, and Y. S. Lee, Synthesis and characterization of single crystals of the spin-1/2 kagome-lattice antiferromagnets $Zn_xCu_{4-x}(OH)_6Cl_2$, *Physical Review B* **83**, 100402 (2011).
- [50] X. Zheng, T. Yamashita, M. Hagihara, M. Fujihala, and T. Kawae, Magnetic transitions in botallackite-structure

- $\text{Cu}_2(\text{OH})_3\text{Br}$ and $\text{Cu}_2(\text{OH})_3\text{I}$, *Physica B: Condensed Matter* **404**, 680 (2009).
- [51] G. M. Sheldrick, Crystal structure refinement with *shelxl*, *Acta Crystallographica Section C Structural Chemistry* **71**, 3 (2015).
- [52] G. M. Sheldrick, Bruker axs area detector scaling and absorption for twinned crystals, University of Göttingen, Germany (2012).
- [53] G. M. Sheldrick, *Sadabs—bruker axs area detector scaling and absorption*, version 2008/1, University of Göttingen, Germany (2008).
- [54] F. Bert, S. Nakamae, F. Ladieu, D. L'Hôte, P. Bonville, F. Duc, J.-C. Trombe, and P. Mendels, Low temperature magnetization of the $S=1/2$ kagome antiferromagnet $\text{ZnCu}_3(\text{OH})_6\text{Cl}_2$, *Physical Review B* **76**, 132411 (2007).
- [55] R. S. W. Braithwaite, K. Mereiter, W. H. Paar, and A. M. Clark, Herbertsmithite, $\text{Cu}_3\text{Zn}(\text{OH})_6\text{Cl}_2$, a new species, and the definition of paratacamite, *Mineralogical Magazine* **68**, 527 (2004).
- [56] M. P. Shores, E. A. Nytko, B. M. Bartlett, and D. G. Nocera, A structurally perfect $s = 1/2$ kagomé antiferromagnet, *Journal of the American Chemical Society* **127**, 13462 (2005), pMID: 16190686.
- [57] D. Chatterjee, *Frustrated magnetism on the anisotropic kagome lattice : a local probe study of Y-kapellasite compounds.*, *Ph.D. thesis*, Université Paris-Saclay (2023).
- [58] E. Fogh, O. Mustonen, P. Babkevich, V. M. Katukuri, H. C. Walker, L. Mangin-Thro, M. Karppinen, S. Ward, B. Normand, and H. M. Rønnow, Randomness and frustration in a $s=1/2$ square-lattice heisenberg antiferromagnet, *Physical Review B* **105**, 184410 (2022).